MNE 15 (2022) 100131

Contents lists available at ScienceDirect

Micro and Nano Engineering

journal homepage: www.sciencedirect.com/journal/micro-and-nano-engineering

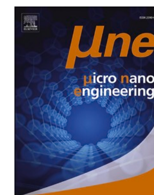

Optimization of an amplification mechanism enabling large displacements in MEMS-based nanomaterial testing devices

Naga Manikanta Kommanaboina [a,b], Maria F. Pantano [a,*], Alvise Bagolini [b,*]

[a] Department of Civil, Environmental and Mechanical Engineering, University of Trento, via Mesiano, 77-38123 Trento, Italy
[b] Fondazione Bruno Kessler (FBK), Micro Nano Facility (MNF), via S. Croce, 77-38122 Trento, Italy

ARTICLE INFO

Keywords:
MEMS
Amplification mechanism
Large displacements
Nanomaterials

ABSTRACT

In this paper we report on the optimization of an amplification mechanism to enable large displacements in microelectromechanical systems (MEMS). As a case study, we considered a MEMS-based platform for the mechanical testing of nanomaterials, but the results we obtained can be extended to other devices, too. The studied device consists of a couple of V-shaped thermal actuators, heat sink beams, comb drives for sensing the displacements delivered by the actuators to the sample to be tested, and an amplification stage capable of amplifying the produced displacements to tens of micrometers. Regarding the amplification stage, three different schemes were designed and simulated in order to identify the optimal solution. To this aim, static structural analyses have been carried out to predict the performance of the amplification mechanism with respect to geometrical parameters, such as inclination angle, length or width of the beams embedded in the amplification stage. An amplification factor as large as 50 is found. The numerical results show good agreement with those obtained from analytical models. The performance of the complete device is also evaluated through 3D steady-state static thermal-electrical analyses under variable voltage applied to the actuators.

1. Introduction

Two-dimensional (2D) materials are layers with one atom or a few atoms thickness, and they have been proved to possess a great potential for the development of a variety of devices, including flexible devices, photoelectronic or electromechanical devices [1]. Graphene was the first discovered 2D material, and after that many other 2D materials have become very attractive, such as transition metal dichalcogenides (TMDCs), black phosphorous (BP), 2D oxides, etc. [2]. In the case of 2D materials, unless they lay onto a substrate [3], it is very challenging to perform mechanical characterization tests. Indeed, it is not possible to apply strain directly by for example pulling or squeezing the material, as typically done for 3D structures, since traditional measurement methods are not suitable for handling 2D material samples due to their atom thickness [4]. In this regard, material testing platforms based on microelectromechanical systems (MEMS) technology resulted to be effective solutions. In general, MEMS include a family of micro-sized electromechanical devices and structures, such as sensors, actuators, energy harvesters, and microgrippers [5,6] which, owing to their small size, are capable of producing force and displacement with high resolution and low power consumption. In the last decades, specific MEMS-based platforms have been proposed capable of applying displacements in a range compatible with nanomaterial sample size (i.e., typically, few micrometers) [7] with high-resolution load and displacement measurement readouts (i.e., μN or nm, respectively) [8]. As small displacements have generally to be delivered and measured, amplification mechanisms based on compliant structures are becoming attractive in MEMS devices, especially when precise motion, high reliability, and accuracy are needed for high sensitivity applications. In many cases, the displacement amplification mechanism uses micro flexures and hinges, as these joints do not have any backlash, and provide repeatable motion. However, these flexures have a limited range of motion [9].

In general, there are different types of amplification mechanisms that were reported in the literature like levers and bridge-type mechanisms [10], which consist of single axis-symmetric circular flexure hinges and V-beam amplification structures [11]. Lai and Zhu [12] designed a lever and bridge-type compliant amplification mechanism consisting of eight rigid bodies connected by ten flexure hinges for piezoelectric drives. In this case, all the flexure hinges were loaded in tension and bending in order to solve potential buckling issues. Ya'Akobovitz and Krylov [9] designed a mechanical amplification mechanism capable of a linear-to-angular motion conversion, which was used for acceleration

* Corresponding author.
E-mail addresses: maria.pantano@unitn.it (M.F. Pantano), bagolini@fbk.eu (A. Bagolini).

https://doi.org/10.1016/j.mne.2022.100131
Received 21 November 2021; Received in revised form 7 March 2022; Accepted 22 March 2022
Available online 26 March 2022
2590-0072/© 2022 The Authors. Published by Elsevier B.V. This is an open access article under the CC BY license (http://creativecommons.org/licenses/by/4.0/).

measurements. Their integrated compliant motion amplifier was able to transform small out-of-plane displacements of a proof mass under inertial forces into significantly larger in-plane displacements. Also, hydraulic displacement amplification mechanisms (HDAMs) have been reported, as shown in [13], for application in tactile displays. In this case, small displacements (i.e., in the order of 10 μm) produced by a piezoelectric actuator are amplified by about 5 times by HDAM. Another type of amplification mechanism is based on the use of cascaded V-beams, as reported in [14] for safety and arming devices. In this case, two amplification stages were implemented. The first amplification stage amplifies the input displacement and pushes a connection mass forward. Simultaneously, the second amplification stage is compressed along the vertical direction while expanding in the horizontal direction. Three different configurations based on compliant-amplification mechanisms were presented by Iqbal et al. [15]. Each configuration consists of two sets of amplification mechanisms placed horizontally. Configuration 1 amplifies the displacement by a factor 9, while in configuration 2 and configuration 3 the displacement is amplified by a factor 17. Iqbal et al. [5] designed a thermally actuated displacement amplification mechanism capable of amplifying displacements by 20 times with comb drives for sensing the displacements. This mechanism operates with thermal actuators output displacements in the x-direction and expands in the y-direction. A mechanical amplification based on V-shaped beams was reported in [16]. In this amplification mechanism, there was neither micro hinges nor flexures involved. The linear behavior of such amplification mechanism was modeled by using the elementary bending theory and it was found as capable of an amplification factor as large as 18.6. The above-described amplification mechanisms need an external force to operate, which can be provided by different types of actuators, such as electrothermal, magnetic, and piezoelectric actuators. Owing to their ease to control, microscale displacements, and forces, the electrothermal actuators are widely used in current MEMS devices, although, they operate at relatively high temperatures, which might limit their applications [17] as, for example, temperature can affect the mechanical properties of a sample to be tested. For this reason, they are often used in combination with heat sink beams, which can limit the temperature increase in the structure [18].

Here, we present the design and optimization of different types of MEMS-based displacement amplification mechanisms in order to enable large displacements in MEMS devices. These amplification mechanisms can potentially be used in platforms for the mechanical characterization of 2D nanomaterials as well in other devices requiring high displacement measurement sensitivity. Our designed MEMS device consists of a pair of thermal actuators, heat sink beams, amplification mechanism, and comb drives for capacitive readout. The desired performance of the device has been considered as follows: maximum displacement delivered by the actuators equal to about 1 μm, temperature increases below 100 °C, capacitive readout sensitivity of about 5 fF/nm. As the MEMS device is intended to be fabricated via a silicon-on-insulator (SOI) fabrication process based on deep reactive ion etching (DRIE), the following design constraints were considered: minimum feature size of all the structures of the device is 4 μm, the minimum gap size is 2 μm, and the device layer thickness is 25 μm.

2. Design of the MEMS platform

All the structures of our MEMS device, namely the thermal actuators, the displacement amplification stage and the displacement capacitive sensor were designed through Solidworks, and finite element (FE) analyses were carried out using the software ANSYS™ Workbench.

2.1. Thermal actuator

The thermal actuator consists of a central shuttle and a number of V-shaped beams with a small flexible hinge at both ends to amplify [19] the delivered displacement (Fig. 1). When a voltage is applied between the anchors of the V-shaped beams, current flows and, by Joule effect, heat is generated causing a temperature increase in the structure, which makes the beams expanding and moving the central shuttle. As the temperature increase can be significant (Fig. 1b) and affect other parts of the MEMS device, like those where a sample will be placed, the thermal actuator temperature needs to be controlled and reduced out of the V-shaped beams. To this aim, we introduced heat sink beams (i.e., to promote heat dissipation by conduction through the substrate) between the V-shaped beams and the location where we expect to have the nanomaterial sample. The results of the electro-thermal analysis reported in Fig. 1 shows that the thermal actuator causes the temperature to increase to 127 °C at the sample location when the actuator is biased with 4 V while delivering the desired displacement of 1 μm.

In order to further decrease the temperature at the sample location while maintaining the delivered displacement of 1 μm, we considered to introduce two thermal actuators placed symmetrically with respect to the nanomaterial sample in a more optimized MEMS device configuration. In this way, it is possible to reach an overall displacement of 1 μm (i.e., half of which delivered by each thermal actuator) while keeping the sample at a constant temperature of 81°C. The possibility to avoid temperature gradients in the sample is also desirable when the MEMS platform is used for strain engineering studies of nanomaterials, thus in combination with other physical characterization techniques that can be very sensitive to temperature variation.

The axial stiffness of each thermal actuator (K_{AC}) can be calculated as reported in [20]:

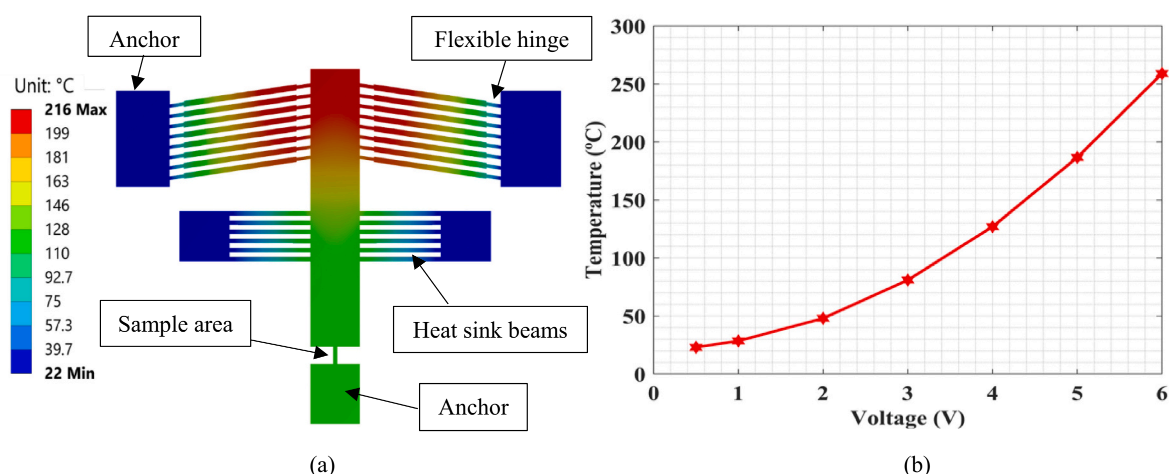

Fig. 1. (a) Thermal actuator maximum temperature when biased with 4 V and temperature variation at the sample location as a function of voltage (b).

$$K_{AC} = \frac{N\,sin^2\theta \times (w_1 + w_2) \times E \times t}{L_{AC}} \quad (1)$$

Where E is the Young's modulus, t is the thickness, L_{AC} is the total length of the actuator beam, N is the number of beams, θ is the inclination angle of the beams, and w_1 and w_2 are the widths of the beam in the thinnest and thickest regions, respectively. Considering the geometrical parameters reported in Table 1. The axial stiffness of our thermal actuators results to be 16,882 N/m. Regarding the heat sink beams, their total stiffness can be calculated as [20]:

$$K_S = 2 \times \frac{N \times E \times b^3 \times t}{L_s} \quad (2)$$

Where, the N is the number of heat sinks (6), L_s is the 200 μm, and width b is 8 μm. The calculated heat sink beam stiffness (K_S) is 3244.8 N/m according to eq. 2.

2.2. Amplification mechanism

In order to measure efficiently the displacements delivered to the sample, we introduced a capacitive sensor to our MEMS device. However, since the displacements involved are very small (up to ≈ 1 μm), we need to sense at least 100 nm. If we consider a standard capacitive measurement scheme, the sensitivity can be computed as [20]:

$$S = \frac{\Delta C}{D} \quad (3)$$

Where, D is the displacement delivered to the sample and ΔC is the capacitive variation produced in the sensor. This latter can be computed as $\Delta C = \frac{2\,N \times \varepsilon \times t \times d}{g}$, where N represents the number of movable comb drive fingers, t is the thickness of the comb-drive fingers, d is the displacement of a finger, g (2 μm) is the gap between fingers, ε is the permittivity of air. In order to achieve a minimum of 5 fF/nm sensitivity and keep a compact footprint, we designed an amplification mechanism able to convert the sub-micrometer displacements delivered to the sample in x50 magnified displacements available at the location where the comb-drive fingers of the capacitive sensor are placed. In order to design such displacement amplification stage two different mechanisms were studied, with the first being based on a V-beam structure and the second one provided with a sigmoidal shape, (Fig. 2). Based on these amplification mechanisms, three schemes of MEMS-based nanomaterial testing devices were considered.

Scheme 1 and 3 devices are designed with a V-beam amplification mechanism, which consists of two flexible beams similar to the previous designs presented in [5,10,12,14,15,21], without the presence of micro hinges. In these schemes, the structure moves in the x-direction when the force is applied, and it expands in y-direction without any rotation to accommodate the x-direction compression (Fig. 3a, c). In scheme 1, the amplification mechanism was directly connected with the thermal actuator central shuttle while in scheme 3 we used elliptical proof masses to connect the amplification mechanism.

In scheme 2 the amplification mechanism takes a sigmoidal shape that consists of thin curved hinges, which are similar to a previous design reported in [22]. In this case, the amplification mechanism is connected to the central shuttle of the thermal actuator by elliptical beams (Fig. 3b). The thin curved hinges (C_1, C_2) rotate in clockwise and counterclockwise directions to provide the rotational displacements. The thin curved beams deflect much more than pseudo rigid bodies S, shown in Fig. 2 (b).

Table 1
Geometrical parameters of the device.

Parameter	Value
Total length of the beam (L_A)	350 μm
Thin beam (hinge) region length	35 μm
Thicker beam region length	280 μm
Width of small beam region (w_1)	6 μm
Width of thicker beam region (w_2)	10 μm
Number of beams pairs	8
Inclination angle	6°
Thickness (t)	25 μm
Heat sink beams ($N = 6$) width	8 μm
Heat sink beam length (L_S)	200 μm
Amplification beams ($N = 4$) width	4 μm
Amplification beam length (l)	800 μm
Amplification beam angle (θ)	1°
Curved hinges (C_1, C_2) radius (R)	50 μm
Curved hinge (C_1, C_2,) width	4 μm

2.2.1. Static structural analysis

3D static structural analyses were carried out to predict the performance of the above-mentioned amplification mechanisms. All the anchor points were mechanically fixed during the simulations and, as constituent material, we considered silicon for all the structures. For silicon, we used the following parameters: Young's modulus, E = 169 GPa, Poisson's ratio (ν) = 0.28, density (ρ) = 2330 kg/m^3.

2.2.1.1. Scheme 1. A static structural simulation was performed under unidirectional load conditions. An input displacement of 0.5 μm was applied to the central shuttle of the thermal actuator along the x-axis and the amplification mechanism resulted to move by 12.2 μm in the direction perpendicular to the applied displacement, as shown in Fig. 3(a). This structure can be used for both in-plane and out-plane displacements in the y-direction. In the case of using it for in-plane displacement, it has some limitations (for example it cannot move more than ≈14 μm) due to the chosen angle of 1°. The amplification mechanism was designed 13.9 μm off from the sample location. A maximum stress of 356 MPa was obtained.

2.2.1.2. Scheme 2. The sigmoidal shape amplification mechanism consists of thin curved hinges C_1, C_2 (shown in Fig. 3b), to reduce their stiffness and enable a rotational movement. When the displacement is delivered by the two symmetrical thermal actuators, forces F_A and F_B are transferred to the thin curved hinges C_1 and C_2, which then rotate around the center of rotation of the thin curved hinge in clockwise and counterclockwise directions, respectively. Meanwhile, the curved hinges C_1 and C_2 develop a rotational output displacement. When a unidirectional input displacement of 0.5 μm is considered as applied by each thermal actuator in the x-direction, this results in an amplified displacement of 4.2 μm at the farthest comb-drive electrodes (shown in Fig. 3b). The total size of the thermal actuator central shuttle has been reduced by 1.5 times in comparison to scheme 1 and has the advantage of reading the displacement at a location much closer to the sample. Furthermore, the maximum stress decreases to 90 MPa.

2.2.1.3. Scheme 3. As scheme 1 resulted as able to provide much higher amplification ratio than scheme 2, we further developed it. In this new configuration, an elliptical proof mass (shown in Fig. 3c) connects the thermal actuator central shuttle to the amplification mechanism. Compared to scheme 1, the use of the elliptical mass allows us to reduce the overall footprint of the device and to increase its stiffness. When an input displacement of 0.5 μm in the x-direction was considered as applied by the thermal actuators, the V-shaped beam experiences an elastic deformation which results in an amplified vertical displacement of 25 μm in the y-direction, as shown in Fig. 3(c); this result is about 2 times higher than the results reported in previous designs [14]–[16,21,23]. A maximum stress of ≈340 MPa was obtained, which is below the usual silicon's yield strength value, namely 7 GPa [24]. From Fig. 3(d), it results that the maximum amplification ratio can be observed in scheme 3, while scheme 2 minimizes the stress concentration with respect to the other schemes due to the presence of the curved hinges of C_1, C_2, as shown in Fig. 3(e).

A parametric analysis was performed to understand the role played by different geometrical parameters on the amplification mechanism of

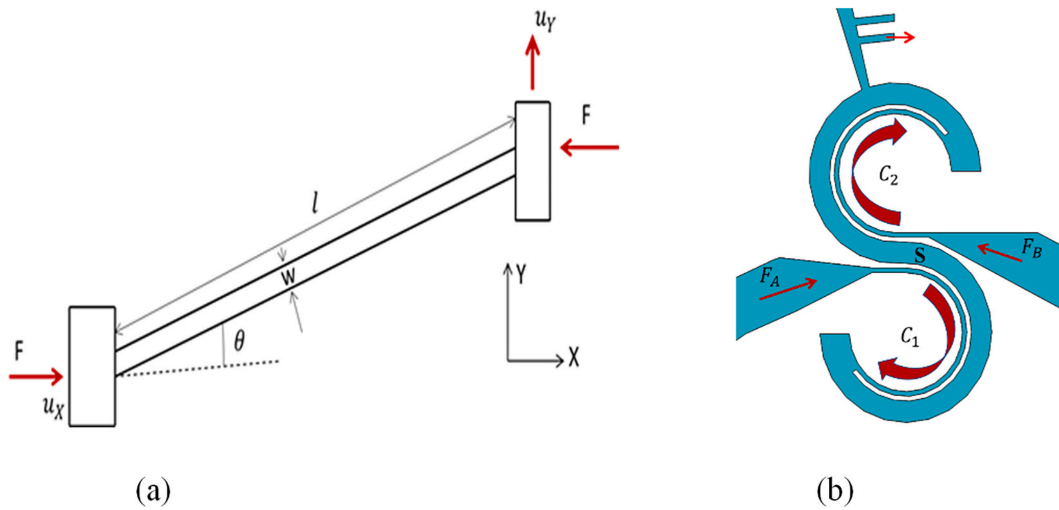

Fig. 2. Schematic diagram of V-beam amplification mechanism (a) and sigmoidal shape amplification mechanism (b).

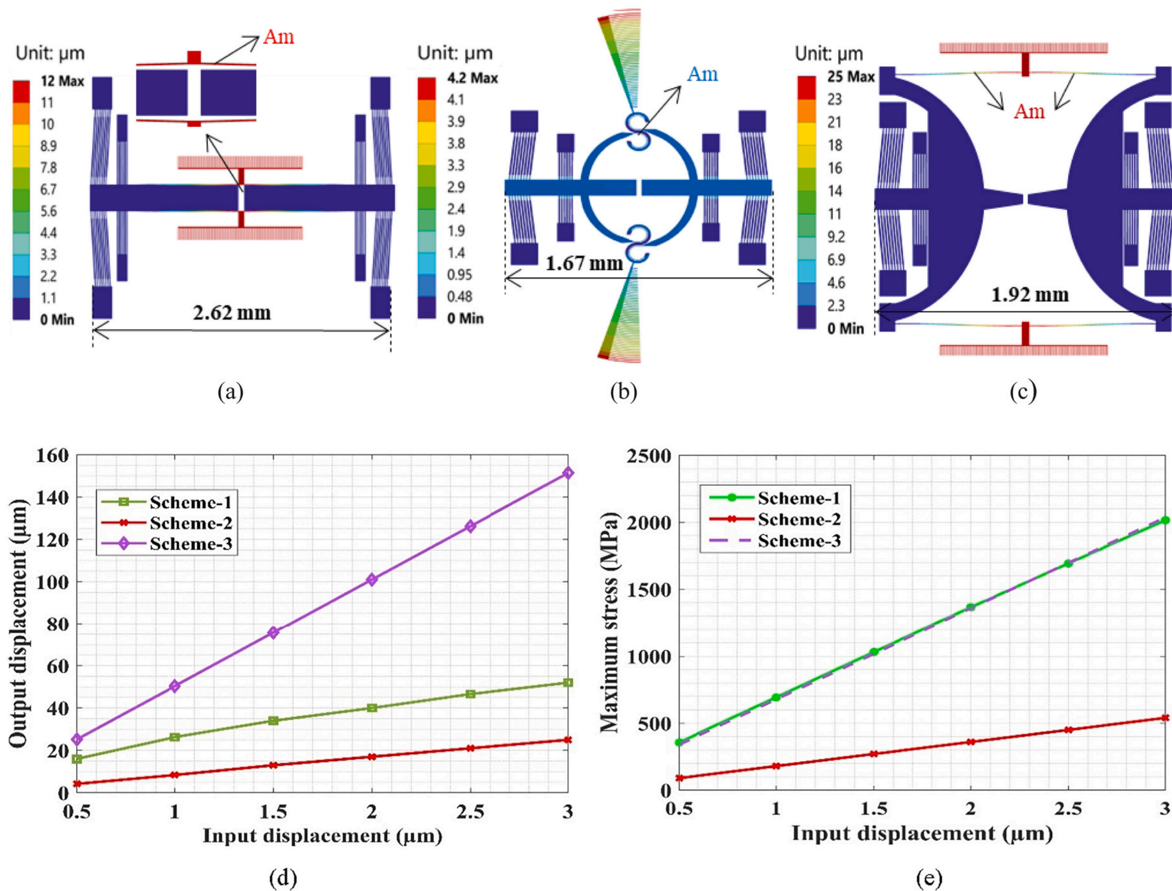

Fig. 3. Displacement field of scheme 1 (a), scheme 2 (b), and scheme 3 (c) when the thermal actuators are moved by 0.5 μm, and performance analysis of the three schemes in terms of (d) output displacement and (e) maximum stress in the total device with respect to the input displacement.

scheme 3. The simulation results show that by decreasing the angle of the V-shaped beam, the amplification factor (i.e., the ratio between the output and the input displacement) increases (Fig. 4(a)). Furthermore, a significant change in the amplification factor results when increasing the flexible beam length, as shown in Fig. 4(b).

From an analytical point of view, the amplification mechanism can be modeled through the elementary theory of bending. By referring to the schematic of Fig. 2(a), which shows the simplified model of one-half of the amplification beam, the deflected amplification beam is subjected to equal and opposite end forces F, along with the couples that prevent the rotation motion. Based on these conditions, the displacement in the axial direction (u_X) and lateral displacement (u_Y) can be calculated as [16]:

$$u_X = \frac{F\cos\theta}{k_A}; u_Y = \frac{F\sin\theta}{k_T} \tag{4}$$

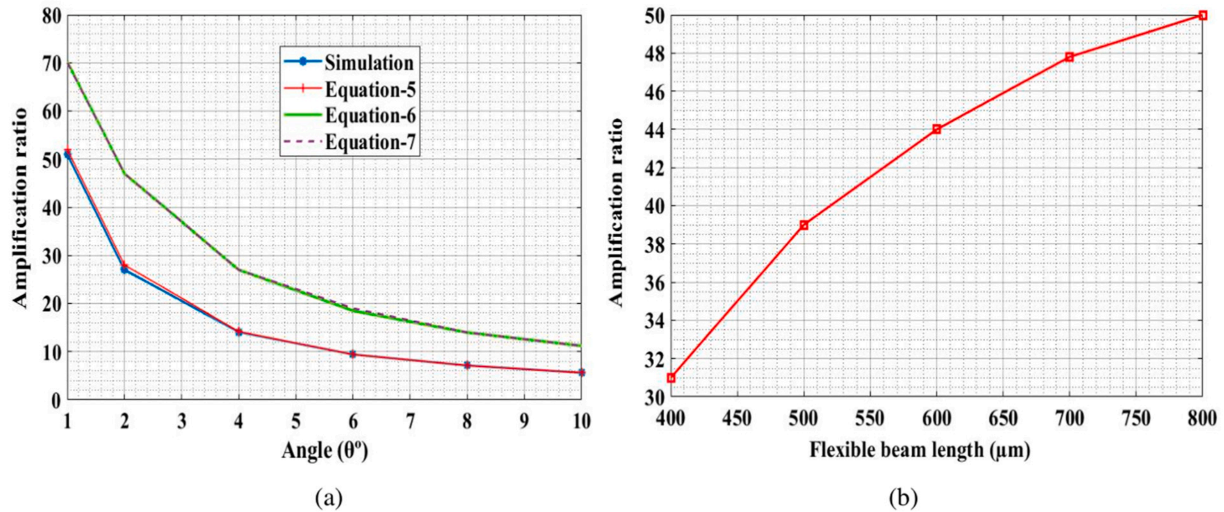

Fig. 4. Amplification ratio comparison with analytical formulas and simulation results with respect to the beam angle (a), and flexible beam length (b).

Where $k_A = \frac{E \times w \times h}{l}$ is the axial stiffness of the amplification beam and $k_T = \frac{E \times w^3 \times h}{l^3}$ is stiffness in the transversal direction, E is the Young's modulus, l is the length, w is the width, θ is the angle of beam, and h is the thickness (25 μm) of the amplification beam. Considering the values reported in Table 1, the axial stiffness of our amplification beam results to be 42,250 N/m. while the transversal stiffness results to be ≈1 N/m. The amplification ratio of the selected mechanism can be calculated as [16]:

$$Am = \frac{\Delta y}{\Delta x} = \frac{1 - \left(\frac{w}{l}\right)^2}{2 \times \left(\tan\theta + \left(\frac{\left(\frac{w}{l}\right)^2}{\tan\theta}\right)\right)} \tag{5}$$

Beyond Eq. (5), in the literature other formulas have been reported [14]–[16] to compute the amplification ratio and output displacements of the V-beam amplification mechanism. For example, in [14], the following model was proposed:

$$Am = \frac{\sqrt{l^2 - (l^*\cos\theta - \Delta x)^2} - l^*\sin\theta}{\Delta x} \tag{6}$$

Where, Δx and l are the input displacement and length of the beam. In [15] the following model was proposed:

$$Am = \frac{l\,(\sin\theta' - \sin\theta)}{U_{input}} \tag{7}$$

Where U_{input} is the applied displacement, $\theta' = \cos^{-1}\left(\cos\theta - \frac{U_{input}}{l}\right)$. Fig. 4(a) shows a comparison between the amplification ratio obtained through Eqs. 5–7 and the one obtained from our simulations. Regarding the geometrical parameters, we used the values listed in Table 1. From Fig. 4(a), it emerges that Eq. (5) proposed by [16] provides the best match with our simulation results with a ≈ 3% maximum difference.

From a structural point of view, safe operation of the devices requires to reduce the magnitude of stresses experienced by all the involved structures, in order to avoid the formation of micro voids that can then result in micro-cracks. Thus, in order to get an insight into the structural integrity of all the three above mentioned device schemes [23], we also computed the safety factor, defined as the ratio between the yield stress and the maximum stress. The calculated safety factor of scheme 3 results to be 20 at the input displacement of 0.5 μm with a maximum stress of ≈340 MPa was obtained. Such a stress level is significantly lower than the yield strength of silicon (7 GPa). According to the static structural results, scheme 3 can be operated safely until 10 μm of input displacement, where the structure is characterized by a maximum displacement of 500 μm and a maximum stress of 6788 MPa.

3. Overall performance of the MEMS device

3.1. Steady state thermal analysis

A multiphysics analysis of the final device configuration (Fig. 5a), consisting of two symmetrical thermal actuators, heat sink beams, elliptical poof mass, type 3 amplification mechanism, sample, and comb drives for displacement capacitive sensing was performed. The following electrical and thermal properties of silicon were considered: thermal conductivity (K) of 130 [W/m·K], coefficient of thermal expansion (α) of 2.6×10^{-6} K^{-1}, and resistivity of 0.005 Ω·cm [25]. The device was actuated by providing a varying bias voltage between the anchor points of the thermal actuators. At 3 V, the displacement delivered at each side of the sample is 0.48 μm in the x-direction, an overall maximum displacement of 22.4 μm is achieved at the comb-drive fingers location (in the y-direction). A maximum temperature of 131 °C was obtained in the device, while a temperature of 81 °C was obtained at the sample location. If the voltage at the thermal actuators increases, this results in higher output displacement, as shown in Fig. 5(b). In the final MEMS device configuration, the displacement at the capacitive readout location was indeed enough to reach the targeted sensitivity of 5 fF/nm with around 1100 number of combs, as previously reported by us [20].

Finally, we performed a modal analysis of the whole MEMS device in order to predict the device natural frequencies, modes and to understand the dynamic response of the device during the excitation [23]. ANSYS Workbench was used to perform the modal analysis and the frequency associated to oscillation in y-direction was about 14.8 kHz, as shown in Fig. 5(c).

4. Conclusions and future work

In order to achieve a deep insight into the mechanical and strain engineering properties of nanomaterials, it is necessary to develop miniaturized testing stages able to apply and measure sub-micrometers displacements. One possibility to improve the resolution of the displacement measurement is to design an amplification mechanism able to magnify the displacements to be recorded. Herein this paper, we analyzed the performance of two different amplification mechanisms, based on either thin curved hinges or a V-shaped beam. As a result of an

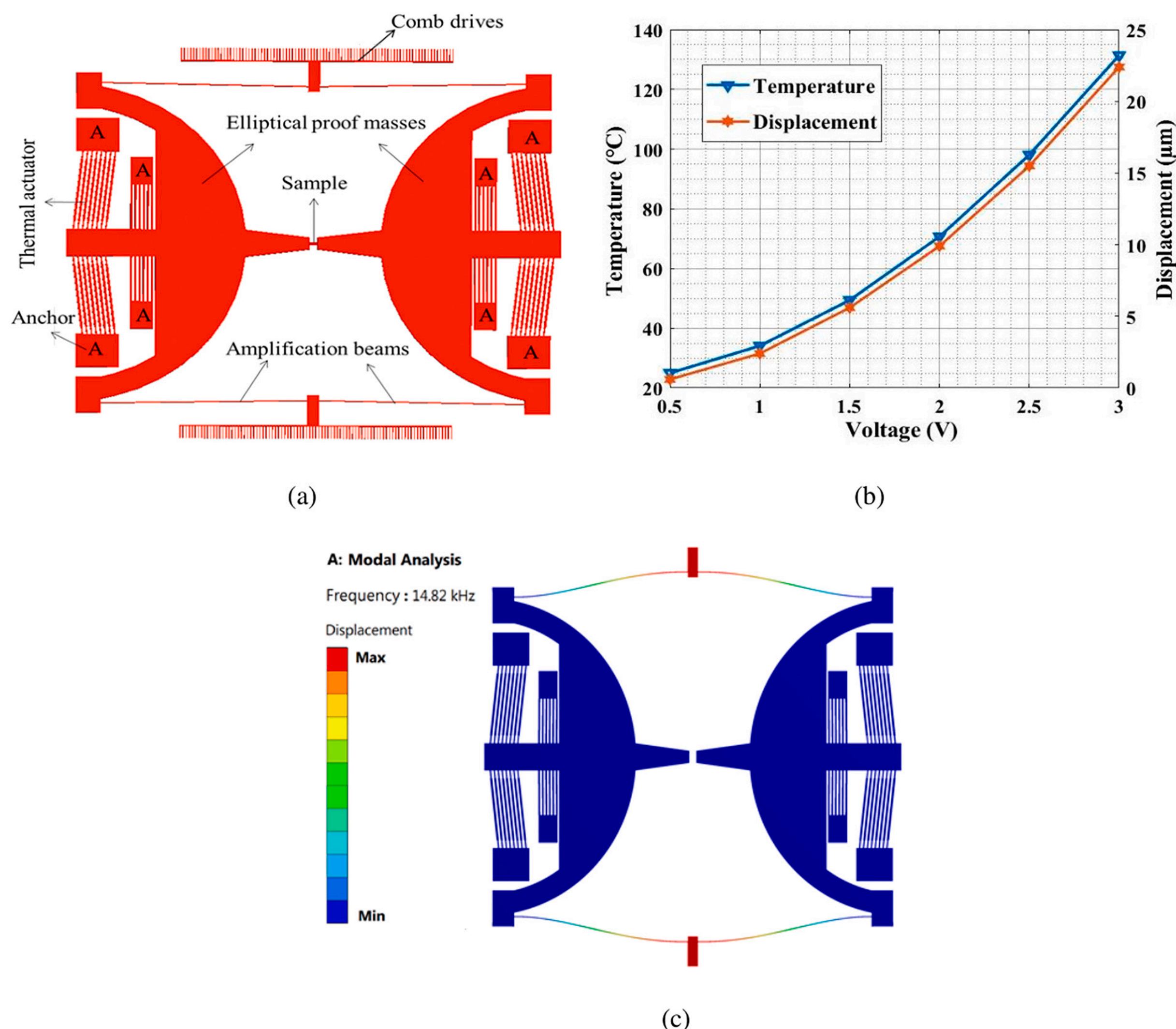

Fig. 5. Final MEMS-based nanomaterial testing device (a), output displacement and temperature of whole device as a function of voltage (b), and modal analysis (c).

optimization process based on FEM analyses, the second mechanism provided the highest amplification ratio, while keeping a compact footprint. Such mechanism was then implemented in the design of a MEMS-based platform for the investigation of the strain engineering properties of nanomaterials. Such platform can deliver displacements to a nanomaterial sample as large as 0.96 μm, which can be magnified by 50 times to improve the displacement measurement resolution, while not overcoming 81 °C at the sample location. The amplification mechanism we designed can in principle be used in other MEMS-based platform for both high-resolution actuation and sensing applications.

Future work will be concerned with the microfabrication of the proposed device by MEMS technology using SOI wafers and deep reactive ion etching process.

Declaration of Competing Interest

The authors declare that they have no known competing financial interests or personal relationships that could have appeared to influence the work reported in this paper.

Acknowledgments

This work has been supported by the project “MONolithic STRain Engineering platform for TWO-Dimensional materials (MONSTRE 2D)” funded by the MIUR Progetti di Ricerca di Rilevante Interesse Nazionale (PRIN) Bando 2017 - grant 2017 Prot. 2017KFMJ8E.

References

[1] N.R. Glavin, C. Muratore, M. Snure, Toward 2D materials for flexible electronics: opportunities and outlook, Oxford Open Mater. Sci. 1 (1) (Nov 2020), https://doi.org/10.1093/oxfmat/itaa002.
[2] Y. Sun, K. Liu, Strain engineering in functional 2-dimensional materials, J. Appl. Phys. 125 (8) (2019), https://doi.org/10.1063/1.5053795. American Institute of Physics Inc., Feb. 28.
[3] J. Cao, et al., Strain engineering and one-dimensional organization of metal-insulator domains in single-crystal vanadium dioxide beams, Nat. Nanotechnol. 4 (11) (2009) 732–737, https://doi.org/10.1038/nnano.2009.266.
[4] M.F. Pantano, I. Kuljanishvili, Advances in mechanical characterization of 1D and 2D nanomaterials: progress and prospects, Nano Express 1 (2) (Sep 2020), 022001, https://doi.org/10.1088/2632-959x/abb43e.
[5] S. Iqbal, A.A. Malik, R.I. Shakoor, Design and analysis of novel micro displacement amplification mechanism actuated by chevron shaped thermal actuators, Microsyst. Technol. 25 (3) (Mar 2019) 861–875, https://doi.org/10.1007/s00542-018-4078-9.
[6] Y. j Choi, S.v. Sreenivasan, B.J. Choi, Kinematic design of large displacement precision XY positioning stage by using cross strip flexure joints and over-constrained mechanism, Mech. Mach. Theory 43 (6) (Jun 2008) 724–737, https://doi.org/10.1016/j.mechmachtheory.2007.05.009.
[7] Y. Yang, et al., Brittle fracture of 2D MoSe2, Adv. Mater. 29 (2) (Jan 2017), https://doi.org/10.1002/adma.201604201.
[8] Y. Zhang et al., “A MEMS tensile testing device for mechanical characterization of individual nanowires,” SENSORS, 2010 IEEE, 2010, pp. 2581-2584, doi: 10.1109/ICSENS.2010.5690164, IEEE, 2010.

[9] A. Ya'Akobovitz, S. Krylov, Toward sensitivity enhancement of MEMS accelerometers using mechanical amplification mechanism, IEEE Sensors J. 10 (8) (2010) 1311–1319, https://doi.org/10.1109/JSEN.2009.2039751.

[10] N. Lobontiu, E. Garcia, Analytical model of displacement amplification and stiffness optimization for a class of flexure-based compliant mechanisms, Comput. Struct. 81 (32) (Dec 2003) 2797–2810, https://doi.org/10.1016/j.compstruc.2003.07.003.

[11] S. Iqbal, A. Malik, A review on MEMS based micro displacement amplification mechanisms, Sensors Actuat. A Phys. 300 (2019), https://doi.org/10.1016/j.sna.2019.111666. Elsevier B.V., Dec. 01.

[12] L.J. Lai, Z.N. Zhu, Design, modeling and testing of a novel flexure-based displacement amplification mechanism, Sensors Actuators A Phys. 266 (Oct 2017) 122–129, https://doi.org/10.1016/j.sna.2017.09.010.

[13] T. Ninomiya, Y. Okayama, Y. Matsumoto, X. Arouette, K. Osawa, N. Miki, MEMS-based hydraulic displacement amplification mechanism with completely encapsulated liquid, Sensors Actuators A Phys. 166 (2) (Apr 2011) 277–282, https://doi.org/10.1016/j.sna.2009.07.002.

[14] X. Li, et al., Design of a large displacement thermal actuator with a cascaded V-beam amplification for MEMS safety-and-arming devices, Microsyst. Technol. 21 (11) (Nov 2015) 2367–2374, https://doi.org/10.1007/s00542-015-2447-1.

[15] S. Iqbal, R.I. Shakoor, Y. Lai, A.M. Malik, S.A. Bazaz, Experimental evaluation of force and amplification factor of three different variants of flexure based micro displacement amplification mechanism, Microsyst. Technol. 25 (7) (Jul 2019) 2889–2906, https://doi.org/10.1007/s00542-019-04313-6.

[16] E. Davies, D.S. George, M.C. Gower, A.S. Holmes, MEMS Fabry-Pérot optical accelerometer employing mechanical amplification via a V-beam structure, Sensors Actuators A Phys. 215 (Aug 2014) 22–29, https://doi.org/10.1016/j.sna.2013.08.002.

[17] D. Hill, W. Szyszkowski, E. Bordatchev, On modeling and computer simulation of an electro-thermally driven cascaded nickel micro-actuator, Sensors Actuators A Phys. 126 (1) (Jan 2006) 253–263, https://doi.org/10.1016/j.sna.2005.09.030.

[18] Q. Qin, Y. Zhu, Temperature control in thermal microactuators with applications to in-situ nanomechanical testing, Appl. Phys. Lett. 102 (1) (Jan 2013), https://doi.org/10.1063/1.4773359.

[19] T. Sitotaw Yallew, M.F. Pantano, and A. Bagolini, Design and Finite Element Analysis of an Electrothermally Actuated Microgripper for Biomedical Applications, 2021 Symposium on Design, Test, Integration & Packaging of MEMS and MOEMS (DTIP), Aug. 2021, pp. 01–06. doi: 10.1109/DTIP54218.2021.9568685.

[20] N.M. Kommanaboina, M.F. Pantano, A. Bagolini, Design and simulation of a MEMS device to investigate the strain engineering properties of 2D nanomaterials, in: 2021 Symposium on Design, Test, Integration & Packaging of MEMS and MOEMS (DTIP), Aug. 2021, pp. 01–06, https://doi.org/10.1109/DTIP54218.2021.9568495.

[21] S. Iqbal, R.I. Shakoor, H.N. Gilani, H. Abbas, A.M. Malik, Performance analysis of microelectromechanical system based displacement amplification mechanism, Iran. J. Sci. Technol. Trans. Mech. Eng. 43 (3) (Sep 2019) 507–528, https://doi.org/10.1007/s40997-018-0213-6.

[22] R. Crescenzi, M. Balucani, N.P. Belfiore, Operational characterization of CSFH MEMS technology-based hinges, J. Micromech. Microeng. 28 (5) (Mar 2018), https://doi.org/10.1088/1361-6439/aaaf31.

[23] S. Iqbal, Y.J. Lai, R.I. Shakoor, M. Raffi, S.A. Bazaz, Design, analysis, and experimental investigation of micro-displacement amplification compliant mechanism for micro-transducers, Rev. Sci. Instrum. 92 (10) (Oct 2021), https://doi.org/10.1063/5.0061820.

[24] K.E. Petersen, Silicon as a Mechanical Material, 1982.

[25] M.F. Pantano, R.A. Bernal, L. Pagnotta, H.D. Espinosa, Multiphysics design and implementation of a microsystem for displacement-controlled tensile testing of nanomaterials, Meccanica 50 (2) (Dec 2015) 549–560, https://doi.org/10.1007/s11012-014-9950-9.